



X-Ray Irradiation-Induced Enhancement of Supercapacitive Properties of Bio-derived Activated Carbon

Rita Kumari¹ · Megha Prajapati^{1,2} · Chhaya Ravi Kant¹

Received: 13 December 2023 / Accepted: 12 March 2024 / Published online: 17 April 2024
© The Minerals, Metals & Materials Society 2024

Abstract

The rising global energy demand calls for the development of highly efficient energy storage devices, particularly supercapacitors with remarkable power density. Because of its high surface area, activated carbon (AC) is crucial as a supercapacitor electrode material. X-ray irradiation of AC leads to modifications in its surface chemistry by altering the sp^2 hybridization of the surface carbons. In the current work, we present x-ray irradiation studies on the supercapacitive properties of AC prepared by adopting an oil wick lamp method using soot derived from waste soybean oil. The activated soot is irradiated at a dose rate of 16 mGy/s under a 60 kV x-ray source and investigated as an electrode active mass for an electric double-layer capacitor (EDLC). The device studies reveal that x-ray irradiation is crucial in determining the sample's physisorption and energy storage properties. The irradiated sample demonstrates high specific power density (135.9 W kg^{-1}) and specific energy density (3.2 Wh kg^{-1}). The energy density of the irradiated AC soot electrode sample is nearly double that of AC, i.e., 3.2 Wh kg^{-1} versus 1.6 Wh kg^{-1} , respectively, making it a potential candidate for efficient electrodes in EDLC devices. The internal resistance of the supercapacitor shows a reduction from 25.5Ω to 24.1Ω after irradiation, thereby increasing the electrode conductivity. The investigations in the current work reveal a significant enhancement of the energy storage capacity of x-ray-irradiated AC for high-performance supercapacitor devices. Moreover, the environmentally friendly methodology adopted to synthesize AC soot can help reduce environmental pollution and contribute to the development of sustainable energy storage devices.

Keywords Irradiated activated carbon · soot · waste edible oil · EDLC supercapacitor

Introduction

As the demand for efficient and sustainable energy storage solutions continues to rise, the quest for enhancing the performance of supercapacitors has led to innovative approaches in materials science.^{1,2} In recent years, the intersection of advanced materials and radiation science has opened up a promising avenue for improving the supercapacitive properties of bio-derived activated carbon (AC)

through x-ray irradiation. Bio-derived AC, renowned for its eco-friendly and renewable nature, possesses a porous structure and high surface area ideal for energy storage applications.^{3–5} Carbon is an optimal material in supercapacitors due to its affordability, lightweight nature, mechanical and chemical stability, abundance, and environmentally friendly characteristics. The energy storage capacity of carbon-based materials stems primarily from electric double-layer capacitance, which arises from the adsorption of ions and charged particles between the electrode and electrolyte. To enhance the specific capacitance of supercapacitors, carbon materials must undergo activation to increase specific surface area (SSA), porosity, and conductivity, which are crucial for electrode performance. Activated carbon finds widespread application in numerous commercial large-scale uses of supercapacitors. These applications span various sectors, such as smart grids and distributed energy storage, hybrid and electric vehicles, energy-efficient industrial machinery,

✉ Chhaya Ravi Kant
chhayaravikant@igdtuw.ac.in

¹ Department of Applied Sciences and Humanities, Indira Gandhi Delhi Technical University for Women, Kashmere Gate, Delhi 110006, India

² Electronics Materials Lab, College of Science and Engineering, James Cook University, Townsville, QLD 4, Australia

marine vessels, wind power facilities, uninterruptible power supplies, power backup systems, and consumer electronics. The activation process involves physical and chemical methods to manufacture electrode materials. However, while ACs typically feature pores within the range of 0.4–4 nm, their wide distribution of pore sizes may limit their effectiveness in specific electric double-layer capacitor (EDLC) applications.⁶

Utilizing biomass-derived AC from biowaste as supercapacitor electrode materials offers sustainable waste management, reducing the environmental impact and promoting a circular economy. By repurposing waste such as edible oil into valuable products, this approach contributes to both environmental preservation and economic viability. Moreover, it fosters innovation and sustainability in energy storage technology, providing a cost-effective alternative to traditional electrode materials and making supercapacitors more accessible.^{7,8}

The controlled application of x-ray irradiation introduces a novel dimension to this field, offering the potential to tailor the structural and chemical characteristics of AC for optimized supercapacitor performance. This exploration of x-ray irradiation-induced enhancements builds upon the well-established principles of AC in energy storage devices. Activated carbon, derived from sustainable sources such as wood, coconut shells, or other biomass, has become a material of choice for supercapacitors due to its exceptional surface area, pore structure, and electrochemical stability.^{8–10} The deliberate exposure of AC to x-ray irradiation introduces a controlled perturbation to its molecular and structural composition, opening avenues for fine-tuning its electrochemical properties. This approach seeks to harness the synergy between advanced materials engineering and radiation science to push the boundaries of supercapacitor technology.

There has been much interest in different types of irradiation on supercapacitor electrode materials, resulting in the reordering of the carbon nanostructure, which leads to improvement in EDLC charge storage.^{11–13} In many early irradiation studies, the treatment and modification of carbonaceous materials was revealed to be a fascinating trend.^{11,14–16} Experiments showed that carbon materials could be modified by microwave, point-beam radiation sources, electron beam, and high-energy gamma (γ) irradiation to tune their various properties. These included increased reaction kinetics, uniform particle distribution, mechanical strength, increased active surface area, and fine-tuning of microcrystalline size, and affected the pore structure of the electrodes.^{13,17,18} Carbon treatment via these irradiation techniques effectively enhances specific

capacitance in the range of 196 F g⁻¹ to 483.2 F g⁻¹ and energy density in the range of 5.6 Wh kg⁻¹ to 17.6 Wh kg⁻¹ by using optimized radiation doses and frequency range and different point-beam radiation sources.^{18–20} Thus, x-ray radiation can be a promising method for modifying and manipulating AC materials to the fabrication of high-performance supercapacitive devices. X-ray irradiation can be an effective technique to increase the specific capacitance (C_{sp}) due to increased specific surface area (SSA), improved conductivity, and optimum pore diameter (P_D) for rapid ion charge transfer.

In this work, we delve into the current state of research at the confluence of x-ray irradiation and bio-derived AC for supercapacitive applications. We explore the key parameters, such as x-ray energy and dose rates that influence the structural modifications of AC. Additionally, we investigate the potential effects of x-ray irradiation on surface functional groups, conductivity, and charge storage capacities, aiming to elucidate the mechanisms contributing to the observed enhancements in supercapacitor behavior. Furthermore, safety considerations and the optimization of irradiation protocols are addressed to ensure the controlled evolution of AC without compromising its integrity.

This interdisciplinary approach holds promise not only for advancing energy storage technologies but also for providing a sustainable and eco-friendly pathway toward optimizing the performance of supercapacitors.²¹ The improper disposal of waste edible oil poses significant environmental concerns globally, leading to issues such as sewer line blockages, water contamination, and ecological deterioration. This study aims to address this issue by repurposing used soybean oil into valuable soot material. Given the necessity for sustainable alternatives and the limited research on waste oil, we focus on extracting AC from waste soybean oil (WSO) using the oil wick method. This method proves to be both straightforward and efficient, yielding soot with high purity and abundance. Soybean oil was chosen for its widespread use in household and commercial cooking applications, highlighting its accessibility and potential for waste conversion into valuable resources.^{22,23} Considering this, we report x-ray irradiation-induced modification of AC characteristics and utilize the irradiated AC for supercapacitor device applications. The device performance was found to be dependent on the dose rate used for carbon irradiation. A dose rate of 16 mGy/s demonstrated outstanding specific capacitance (93.56 F g⁻¹) as compared to the untreated AC (51.35 F g⁻¹), with high energy density (3.28 Wh kg⁻¹) and power density (135.90 W kg⁻¹). By unraveling the intricacies of x-ray irradiation-induced modifications in bio-derived AC, researchers can develop next-generation supercapacitors with superior energy density, enhanced charge/discharge rates, and sustained cycle life.

Experimental Details

Materials Used

Activated carbon (used cooking soybean oil, Fortune Foods) was obtained using the oil wick method. PVDF-HFP (polyvinylidene fluoride-co-hexafluoropropylene, 99.9% purity, Sigma-Aldrich), 1-methyl-2-pyrrolidone (NMP, 99.5% purity, CDH), and carbon black (Super P, conductive, 99.9% purity, Alfa Aesar) were used in this study. Graphite sheets (Nanoshel) of 0.5 mm thickness were used for the deposition of slurry, and sodium hexafluorophosphate (NaPF₆, 99.9% purity, Sigma-Aldrich) was used as the electrolyte. Hydrochloric acid (HCl) assay (30%) and deionized (DI) water were used for washing, and Whatman filter paper (0.5 M NaPF₆) was used as a separator between the two symmetrical electrode devices.

Synthesis and X-Ray Irradiation of Activated Carbon

Soot was collected on a stainless steel (SS) plate using incomplete combustion of waste cooking soybean oil from the flames of an oil wick lamp in an air environment (Fig. 1). In the next step, a mixture of soot and KOH in a ratio of 1:2 was mixed in a mortar and pestle for 30 min. The mixture was transferred into an alumina crucible boat and placed into a tube furnace for activation (10°C/min and 850°C). The reaction lasted 1 h while maintaining an inert (N₂) atmosphere, with further cooling to ambient temperature. The resulting prepared powder was washed multiple times with 1 M HCl aqueous solution, followed by DI water, to obtain a pH of 7 in order to enhance the pores in the carbon framework. Finally, the solid residue was filtered and oven-dried at 60°C for 10 h to obtain the AC powder.

In the second step, AC was exposed at a dose rate of 16 mGy/s under 60 kV using a dental x-ray machine as the source. Radiation doses are measured in the unit “gray” (Gy), where 1 Gy equals the joule absorbed per kilogram of

sample. The dose rate of the x-ray source was determined by Eq. 24:

$$D = \frac{g * (kV)^2 (mA) * s}{d^2}$$

Here, D is the x-ray dose rate, g is a constant with a value of 0.043, kV is tube voltage, mA is tube current, s is x-ray exposure time in seconds, and d is the distance of the source from the detector (cm).

Fabrication of AC Electrode

A weight ratio of 8:1:1 for AC, PVDF-HFP, and carbon black (super P) was used to create the slurry for the electrodes. Firstly, the binder (PVDF-HFP) was stirred in NMP for 30 min, and AC and carbon black were added to form a uniform slurry. For the fabrication of electrodes, the prepared slurry was uniformly drop-cast onto a graphite sheet (10 × 10 × 0.5 mm). The prepared electrodes were then vacuum-dried at 80°C overnight in an oven. The deposited active mass on each single graphite electrode was ~0.0012 g and 0.0011 g for AC and x-ray-irradiated AC, respectively. The EDLC symmetrical device was constructed by making a sandwich formation of two AC electrodes and then using a dipped Whatman filter paper as a separator (0.5 M NaPF₆) electrolyte.

Material Characterization

Characterization of the samples (AC, x-ray-irradiated AC) was performed at room temperature. X-ray powder diffraction (XRD) data were obtained on a fifth-generation MiniFlex 600 (Rigaku, Japan). To investigate the functional groups, KBr and both prepared samples were uniformly mixed in a ratio of 1:1000 using an agate mortar and pestle, and pellets were formed by applying pressure (50 MPa) for 1 min using Fourier transform infrared spectroscopy (FTIR; Shimadzu, Japan). The morphology of the prepared sample was acquired using field-emission scanning electron microscopy (FESEM; Nova NanoSEM-450). The pore size and surface analyses were conducted using Brunauer–Emmett–Teller (BET) theory in a Novatouch 4LX gas (N₂) sorption analyzer (Anton Paar/Quantachrome, Austria). X-ray irradiation of AC was conducted using a commercially available low-energy source, intraoral dental x-ray setup (60 kV tube voltage, 30 keV photon energy, 8 mA tube current, 3 s pulse width). The electrochemical studies were performed using a potentiostat (Autolab, USA) for the two-electrode sandwich-configured symmetrical device setup and included cyclic voltammetry (CV), Nyquist plots, and galvanostatic charge/discharge (GCD) cycle tests.

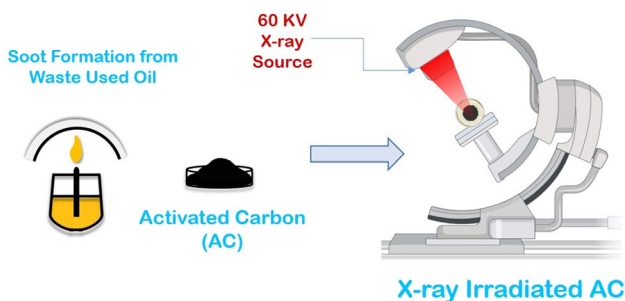


Fig. 1 Schematic of bio-derived activated carbon and x-ray-irradiated AC.

Activation Mechanism

The activation mechanism starts with a solid (carbon)–solid (KOH) reaction, followed by a solid–liquid reaction in which the K^+ ion is reduced to form metallic K, and carbon is oxidized to carbon oxide and carbonate. The main byproducts H_2O , CO_2 , CO , H_2 , K_2O , and K_2CO_3 are formed during activation below $700^\circ C$.²⁵



The formation of H_2O in Eq. 1 is combined with carbon in the activation process to form CO and H_2



CO formed in Eq. 2 is combined with CO to form CO_2 and H_2



Equations 2 and 3 indicate porosity formation via carbon gasification.



The formation of K_2CO_3 occurs above $400^\circ C$, and KOH is wholly consumed at above $600^\circ C$. Potassium carbonate (K_2CO_3) is formed and then breaks into CO_2 and K_2O at above $700^\circ C$, completely disappearing at $800^\circ C$, as shown in Eqs. 4 and 5.



The resulting CO_2 is reduced into CO and K and can also be reduced by carbon to make metallic K at above $700^\circ C$, as shown in Eqs. 6, 7, and 8.

In conclusion, there are mainly two processes during the etching of the carbon framework for generating a porous network: firstly, chemical activation by redox reaction between the chemical activating agents (KOH) and carbon, and secondly, gasification through the formation of H_2O and CO_2 by physical activation.²⁶

Results and Discussion

Functional Groups and Structural Analysis: FTIR and XRD

X-ray powder diffraction (XRD) analysis, shown in Fig. 2a, identified broad peaks that indicate the formation of amorphous carbon. Two broad XRD peaks were identified in the 2θ range of 20° to 45° , with peak maxima at 25° and 43.6° corresponding to (002) and (100) peaks of AC samples.²²

The different functional groups/vibration peak positions are shown in the FTIR spectra of AC and x-ray-irradiated AC (Fig. 2b). The wide peak at 3326 cm^{-1} is assigned to the O–H stretching vibration peak primarily because of the adsorbed moisture in the prepared sample.^{27,28} The 2930 cm^{-1} and 2856 cm^{-1} peaks occurred due to C–H stretching (CH_3 , CH_2 , and CH) observed in both prepared samples.²⁹ The peak intensity at 1741 cm^{-1} is enhanced in the AC sample after x-ray irradiation, indicating that nitrogen predominantly exists in the N–C=O functional group. It has been reported that the functional group of nitrogen in the prepared sample may be a reason for the improved electrode

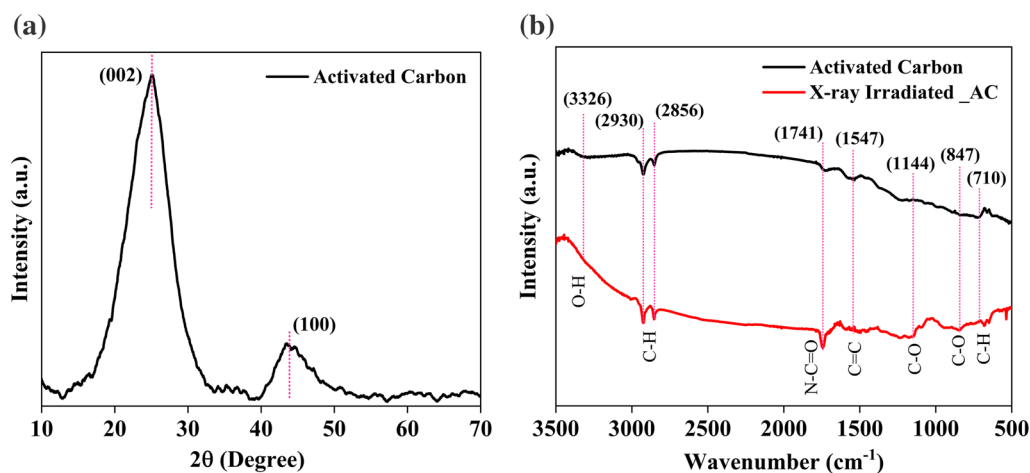


Fig. 2 XRD patterns. (a) Activated carbon (AC); (b) FTIR transmittance spectra of AC and x-ray-irradiated AC.

capacitance.³⁰ The aromatic rings occurred due to vibrational C=C group stretching, giving rise to a 1547 cm^{-1} peak and are more pronounced in AC. The peaks at 1144 and 847 cm^{-1} occur because of C–O stretching and are more prominent in this wavenumber range due to the x-ray-irradiated AC. The peak intensity at 1741 cm^{-1} is enhanced in the AC sample after x-ray irradiation, indicating the N–C=O functional group, and the peaks at 1144 cm^{-1} and 847 cm^{-1} occur because of C–O stretching and are more prominent in this wavenumber range due to x-ray-irradiated AC as shown in Fig. 2b. An enhancement of oxygen-containing functional groups was observed after the irradiation of the AC sample. This phenomenon may occur due to the addition of oxygen ions to the double bonds in the graphitic carbon layers, and reactions of the species with the surface functional groups are observed at a radiation dose of 16 mGy/s in the intensities of planes (002) and (100), respectively.³

Morphological Studies

Morphological studies of the AC and x-ray-irradiated AC samples were carried out using FESEM. When the activation temperature was above 800°C , a porous carbon network occurred due to the activation process (Fig. 3a–d). FESEM micrographs (Fig. 3a, b, c, d) corresponding to AC and x-ray-irradiated AC, respectively, depict a well-defined morphology with uniform spherical mesopores (2–50 nm)

and macropores (50–80 nm), and the narrow pore size was confirmed by the pore size distribution as shown in the inset micrograph. Figure 3a shows consistent grainy morphology with a well-defined spherical structure. Enhanced porous structures with well-defined alleys were formed after x-ray irradiation (Fig. 3b, d). These alleys and enhanced mesoporous structures offer a high surface area, providing superior accessibility to the electrolyte ions for EDLC formation, enabling better electrochemical performance.³¹ The AC sample maintained connectivity between the grainy morphology of all particles after irradiation, which helped enhance the electrical conductivity.

Surface Area and Pore Size Distribution Analysis

BET is a gas physisorption technique on a solid surface. The BET findings of both samples are presented in Fig. 4, and the observed values are listed in Table I. The monolayer gas volume adsorbed by the solid AC powder samples gives the total surface area, and the pre volume and pore size distribution were estimated with the help of BET. The nitrogen physisorption isotherms (IV type) carried out at 77 K are shown in Fig. 4a, b for both AC and x-ray-irradiated AC samples, which arises for samples having both pore size distribution ranges, i.e., mesopore and micropore radius. Gas molecules (N_2) interact with the sorbent mesopore surface, indicating capillary condensation, which causes the path

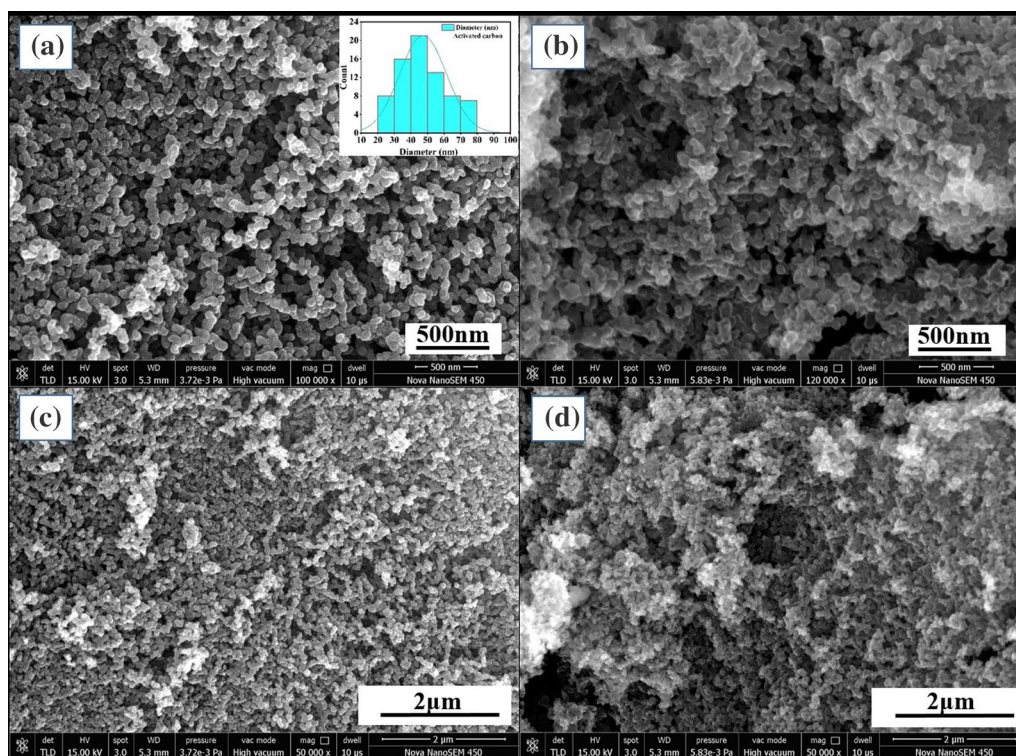


Fig. 3 FESEM micrographs. (a, c) Activated carbon (AC) and (b, d) x-ray-irradiated AC.

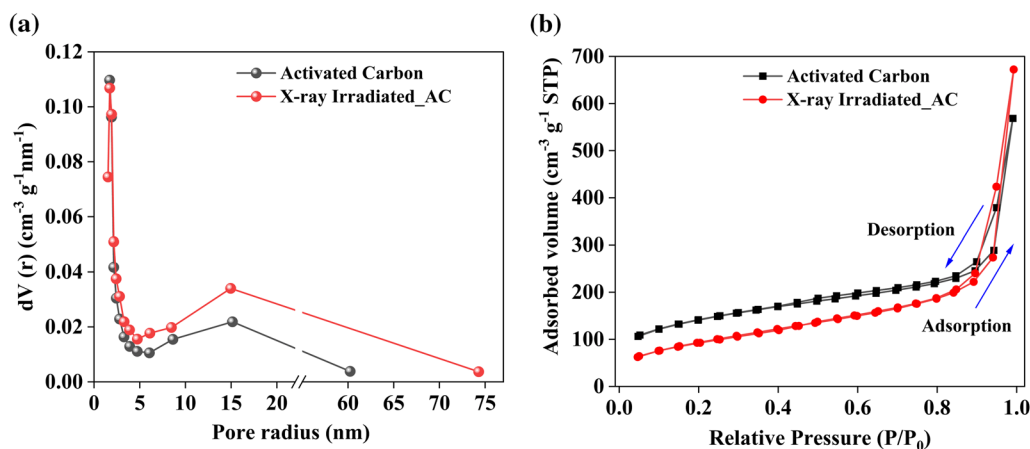


Fig. 4 BET. (a) Pore size distribution curves using the Barrett–Joyner–Halenda (BJH) method. (b) Nitrogen adsorption/desorption isotherm.

Table I Physisorption and electrochemical performance parameters for both samples

Sample	Surface area (SA) ($\text{m}^2 \text{g}^{-1}$)	Pore diameter (P_D) (nm)	Internal resistance (Ω) (R_{in})	Specific capacitance (F g^{-1}) at 0.4 Ag^{-1}
AC	514.01	4.36	24.11	51.35
X-ray-irradiated AC	578.86	5.68	25.50	93.56

difference during adsorption and desorption for dissimilar types of hysteresis loops,³² as shown in Fig. 4b.

The hysteresis loop (H1 type) confirms the spherical shape of the pores.³³ The surface area (SA) and pore diameter (P_D) of AC and x-ray-irradiated AC are $514.01 \text{ m}^2 \text{g}^{-1}$, $578.86 \text{ m}^2 \text{g}^{-1}$, and 4.36, 5.68 nm, respectively, as listed in Table I. Micro- and mesoporous surfaces typically have a large surface area, which improves electrolyte diffusion and increases the supercapacitor's specific capacitance results best aligned with FESEM pore size distribution.³⁴ However, the pore size distribution curve of x-ray-irradiated AC shows wide pore diameters ranging from 1.4 nm to 70 nm and peaking at 1.74 nm and 14.94 nm. Thus, x-ray-irradiated AC is classified as a mesoporous material, which is strongly preferred in electrochemical devices. This is a desirable condition for electrolyte ions to penetrate the electrode's active mass for the formation of an EDLC device to give rise to enhanced electrochemical performance.

Electrochemical Characterization

The performance parameters of the two-electrode, symmetrical EDLC cells fabricated with AC and x-ray-irradiated

AC as electrodes were studied using CV, GCD, and Nyquist plots (electrochemical impedance spectroscopy) on an electrochemical workstation.

Specific capacitance (C_{sp} ; F g^{-1}) was estimated from the discharge time (s) of the GCD curve using well-known electrochemical equations^{22,35}:

$C_{sp} = \frac{2I\Delta t}{m\Delta V}$ where m is the active mass (g) on one symmetrical electrode, I is current density, ΔV is the cell voltage, and Δt is discharge time.

The energy density and power density (E_d , Wh kg^{-1} ; P_d , W kg^{-1}) by using the following equations:

$$E_d = \left[\frac{C_s}{(8 \times 3.6)} (\Delta V_{\max})^2 \right]; \quad P_d = \frac{[Ed \times 3600]}{\Delta t}$$

Here, ΔV_{\max} is a symmetrical cell operational voltage window.

The CV curves of the fabricated symmetrical cell device within the potential window range (0–1 V) at different sweep rates from 10 mV s^{-1} to 100 mV s^{-1} are shown in Fig. 5a. An ideal rectangular shape of the EDLC charge storage mechanism is evident at all sweep rates for AC and x-ray-irradiated AC samples. Exposure to x-rays induced both minor and major alterations in sample porosity and pore network, leading to changes in the AC sample. The evenly distributed microporous microstructure within the network of open pores throughout the samples presents favorable avenues for enhancing the charge storage capacity of carbon-based electrode materials.¹³ The reversibility of the symmetrical electrode active mass on a cell was confirmed by the similar rectangular shape of the CV curves with increasing scan rate.³⁶ Maintaining a nearly rectangular shape at high sweep rates up to 100 mV s^{-1} validates the good rate capability of the electrodes. The area under the curve and voltammetric currents increase gradually with the sweep rate.³⁷ The AC irradiated with 16 mGy/s at a scan rate of 100 mV s^{-1} , as

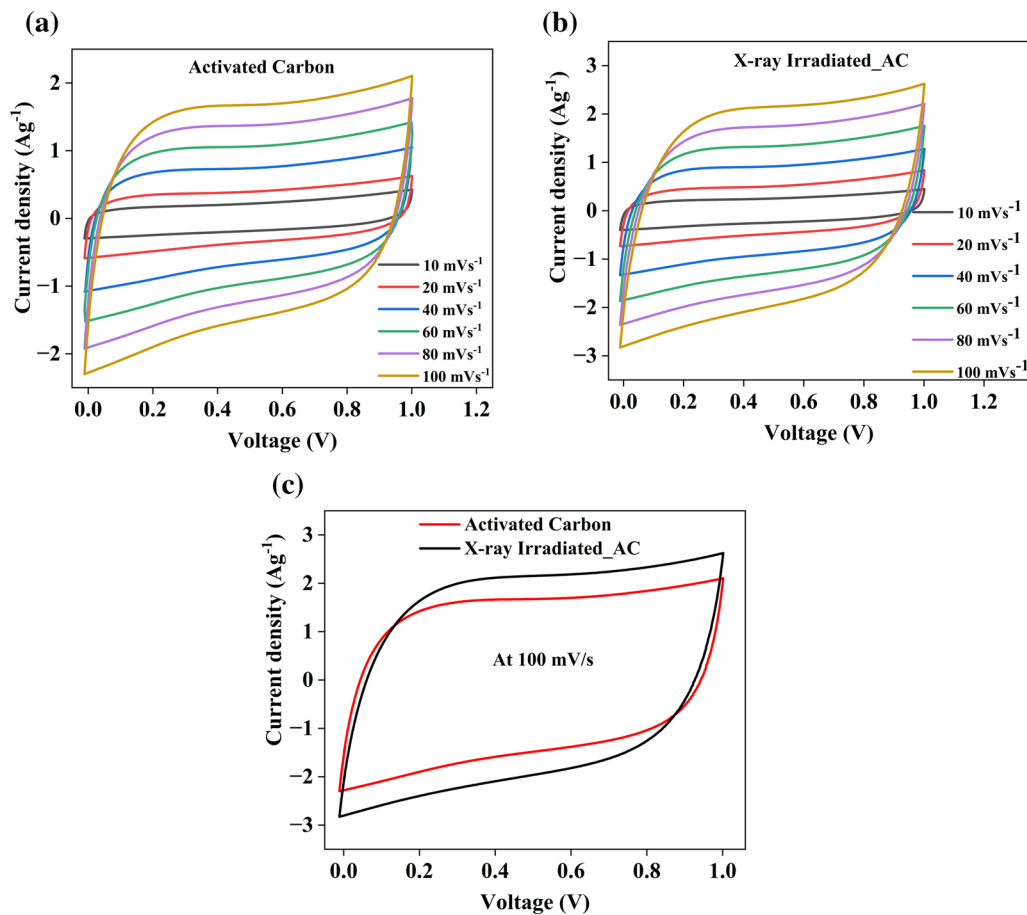


Fig. 5 Cyclic voltammogram. (a, b) CV measurements at different sweep rates and (c) comparative CV curves at 100 mV s⁻¹ for both samples.

shown in Fig. 5c, showed the best rectangular shape compared to those without irradiated AC, signifying capacitive behavior. Hence, the irradiated AC sample gives the highest specific capacitance (C_{sp}) compared to the AC samples. This indicates considerable capacitive performance enhancement, further confirmed by GCD curves shown in Fig. 6.

The specific capacitance (C_{sp}) of AC and x-ray-irradiated electrode material were found to be 51.35 F g⁻¹ and 93.56 F g⁻¹ at 0.4 A g⁻¹ current density. Irradiated AC electrodes exhibited a longer discharge time (Δt) (Fig. 6a), indicating higher charge storage capacity than AC, supported by CV analysis. The enhancement in specific capacitance by x-ray irradiation compared to AC devices might be due to the improved conductance because of induced irradiation charges.³⁸ Furthermore, the increased capacitance observed in the x-ray-irradiated sample can be linked to its increased surface area, enhanced porosity, and more dispersed pore size distribution morphology of the carbon electrodes. These factors facilitate rapid electrolyte transport and efficient ion diffusion, contributing to the increased capacitance values.¹⁶ The specific capacitance decreases gradually with the increase in current density, which can be attributed to

the limited transport of the electrolyte ions into the pores of the electrode's active mass.^{39,40} The high capacitance value is due to the spherical porous morphology of the AC electrodes after x-ray irradiation, which allows the rapid transport of the diffused electrolyte ions. Physisorption and electrochemical performance parameters for both samples are listed in Table I.

Nyquist plots were recorded over a frequency range of 0.001 to 10⁵ Hz for the AC-based supercapacitor symmetrical cells, which are given in Fig. 7a. Over the high- to low-frequency range, the sum of intersections of the origin of the semicircle arc with real impedance and a small semicircle (electrolyte resistance) denotes the internal resistance (R_{in}) which includes the interfacial resistance between the active material and current collector, internal resistance of the electrolyte, electrode material, and collector.^{41,42} A lower internal resistance (R_{in}) value is observed in the x-ray-irradiated AC than in the AC sample, i.e., 24.11 Ω versus 25.50 Ω , respectively, indicating enhanced conductivity, fast electron transfer kinetics, and high electrochemical activity in AC after x-ray irradiation. The reduction in internal resistance can be ascribed to the improved electrical conductivity of

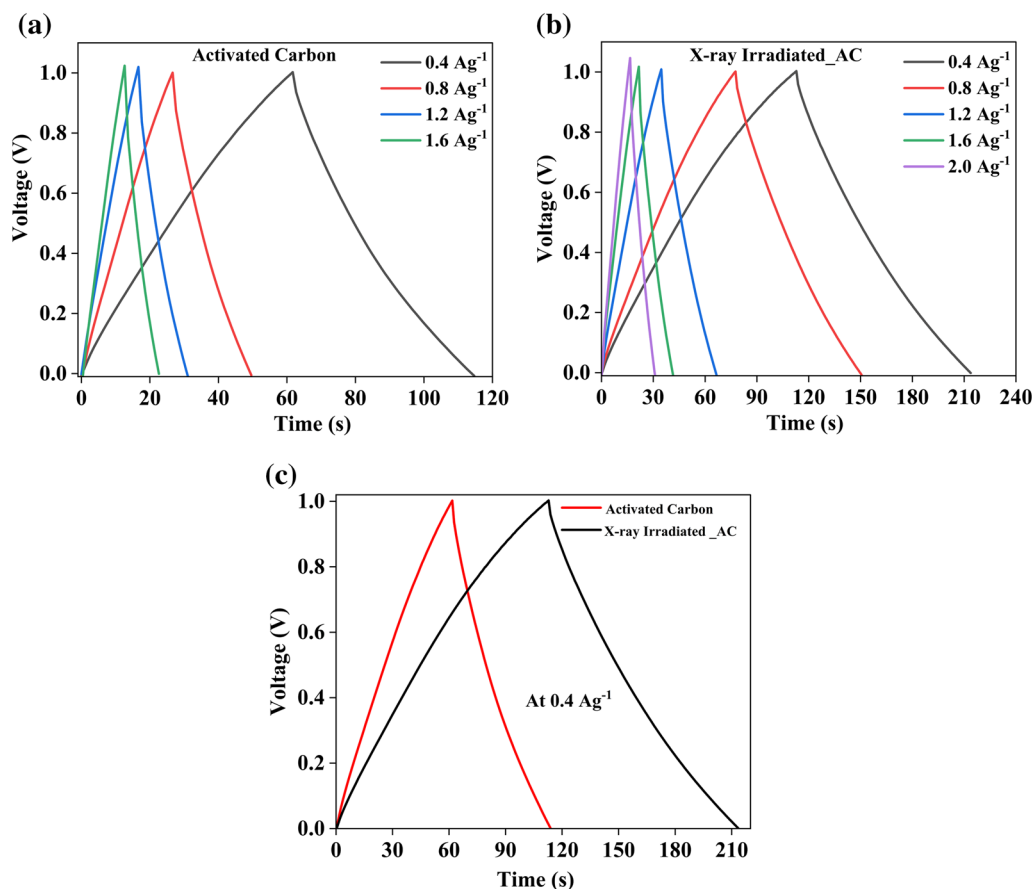


Fig. 6 Galvanostatic charge/discharge. (a, b) GCD measurements at different current densities and (c) comparative GCD curves at 0.4 A g⁻¹ for both samples.

the AC, as irradiation induces significant alterations in the arrangement of sp² states due to the tunneling of charge carriers through adjacent conductive chains.⁸ However, at mid-frequency, a Warburg diffusion line (straight line with a slope of approximately 45°) is observed, which signifies the combination of capacitive and resistive behaviors of the electrolyte ions penetrating the pores of the electrode's active mass, and at low frequency, the capacitive line region (parallel to the imaginary axis) further confirms the capacitive nature of the electrodes, given by $Z'' = \frac{-1}{jCw}$, where w is the angular frequency and C is the capacitance.^{43,44} Compared to AC, the steeper rise in the curve after the semicircle observed in the x-ray-irradiated sample indicates the formation of the electric double-layer system at the electrode/electrolyte interface.¹³ The inset in Fig. 7a shows the semicircular graph at the high-frequency range of the Nyquist plot. The Nyquist plots of the x-ray-irradiated AC samples show better charge transfer than AC.

The maximum energy and power density of the x-ray-irradiated electrode were 3.2 Wh kg⁻¹ and 135.9 W kg⁻¹ at 0.4 A g⁻¹ current density, with 87% retention compared

with AC of 79% after 2200 GCD cycles at 1 A g⁻¹ (Fig. 7b), suggesting the good retention capacity of the symmetrically configured device. It takes nearly 32 h to test the stability of GCD charging and discharging cycles at a potential value of 1 A g⁻¹. A bar graph comparing these results with previously reported work using different irradiation sources is shown in Fig. 7c. The CV plots with changing dose rates from 16 mGy/s to 80 mGy/s show better performance at 16 mGy/s, as seen in Fig. 8a. Irradiation at higher doses of 48 mGy/s and 80 mGy/s led to deterioration in performance with increased asymmetry in the curve, possibly due to structural distortion caused by the x-ray irradiation. This is also evident from the FESEM results, which show a wide mesoporous range. The CV results show the same trend as a two-electrode device, where better electrochemical energy density (3.2 Wh kg⁻¹) and power density (136 W kg⁻¹) were observed at the optimum dose rate of 16 mGy/s, as seen in the plot in Fig. 8b. Bombardment at lower doses may lead to structural realignment and restructuring of defects in x-ray-irradiated AC to assist charge trapping and storage. Therefore, the bombardment of the optimum dose (here, 16 mGy/s) of

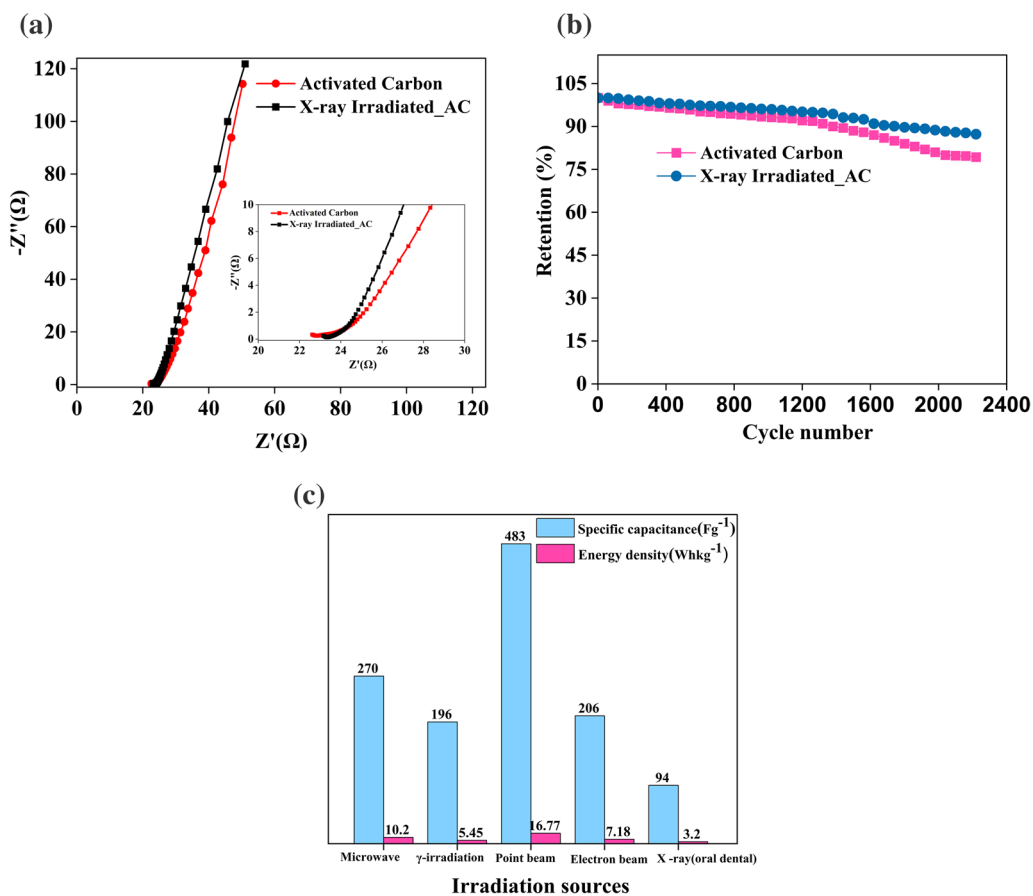


Fig. 7 (a) Nyquist plot in the frequency range of 0.001 to 10^5 Hz for both samples. (b) Retention (%) with number of cycles for AC and x-ray-irradiated AC samples. (c) Bar graph comparing the results with previously reported work.

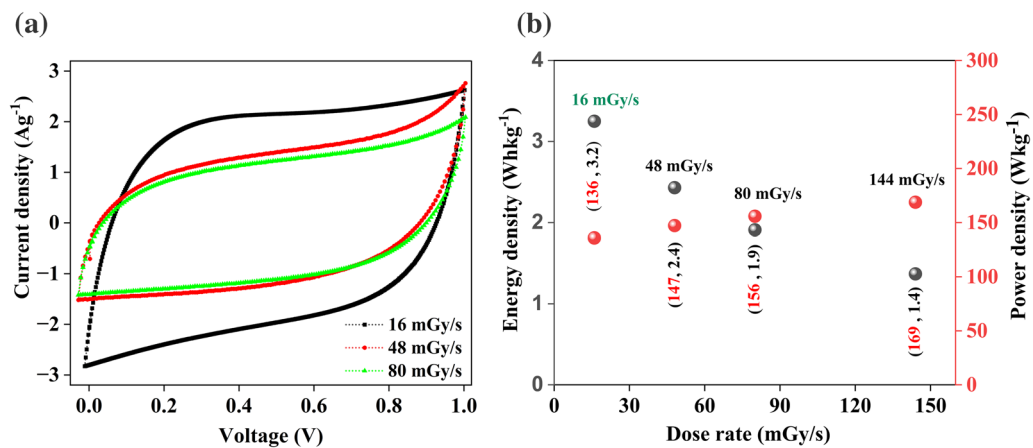


Fig. 8 (a) CV plots at different dose rates. (b) Comparative graph of energy and power density values at optimum 16 mGy/s with higher dose rates.

energetic ion beams (x-ray irradiation) has led to structural changes and thus to enhanced charge storage ability of the AC soot, benefiting the electrochemical performance of supercapacitor devices. This study innovatively

repurposed used soybean oil into valuable soot material and investigated the supercapacitive properties via x-ray irradiation. This unique method involves synthesizing AC using soot from recycled waste soybean oil through an oil

Table II Comparative table of electrochemical performance parameters using different irradiation methods

Irradiation source	Radiation (dose/dose rate/power)	Sample (electrolyte)	Specific capacitance (F g ⁻¹)	Energy density (Wh kg ⁻¹)	Life cycle (retention %)	References
Microwave irradiation	2.45 GHz, 900 W	(NiO)/(NiO@rGO) (6M KOH)	270/395 (1.0 A g ⁻¹)	10.2/17.55	–	19
γ-irradiation	5 kGy	Oil palm fiber (6 M KOH)	196 (10 mA cm ⁻²)	5.45	–	13
Point-beam radiation	Na-22, Co-60, Sr-90, and Am-241	Graphite-based (3M H ₂ SO ₄)	483.20 (0.2 A g ⁻¹)	16.77	5000 (97.4)	18
Electron beam	50–360 kGy	rGO (6MKOH)	206.8 (0.2 A g ⁻¹)	7.18	1000 (42.8)	20
X-ray (Oral dental)	16 mGy/s	Waste soybean oil (Soot) (0.5 NaPF ₆)	93.56 (0.4 A g ⁻¹)	3.25	2200 (87.0)	This work

wick lamp process, offering a sustainable waste management solution. With limited research on waste edible oil utilization, this approach taps into the widespread household and commercial use of soybean oil, demonstrating its potential for transforming waste into valuable resources and advancing environmentally friendly practices and circular economy initiatives. Also, a comparison of electrochemical performance parameters using different irradiation methods is shown in Table II.

Conclusion

X-ray irradiation and dose rate strongly affect the surface area, pore diameter, and mesoporous range of irradiated AC. Surface modification via x-ray irradiation dramatically improves the wetting behavior of the porous AC (soot) and creates capacitance through a combination of electric double-layer formation. AC from waste soybean oil and x-ray-irradiated AC were investigated for supercapacitor electrode applications. A dose rate of 16 mGy/s induced significant changes in the morphological structure of the irradiated ACs, which affected the porosity and network of pores produced in the AC during treatment. A low dose of x-ray irradiation was found to be optimum for the wide mesoporous range, which significantly affected electrolytic ion accessibility and surface characteristics, enhancing the performance of supercapacitors. The morphological studies of the AC irradiated by x-rays shows well-defined morphology with uniform spherical mesopores (2–50 nm) and macropores (50–80 nm) that offer a high surface area of 578.68 m² g⁻¹, confirming superior accessibility to the electrolyte ions for EDLC formation needed for high electrochemical performance. The specific capacitance of the irradiated AC soot electrode sample almost doubled that of AC, i.e., 93.56 F g⁻¹ versus 51.35 F g⁻¹, respectively. Moreover, the stability of the x-ray-irradiated AC device was enhanced by 9%, with

retention of 87% compared with AC (~79%) after 2200 GCD cycles at 1 A g⁻¹. Thus, the x-ray dose rate is a crucial factor influencing the energy storage capacity of carbon material. This study favors the x-ray irradiation method, a simple and effective approach for modifying bio-derived AC in fabricating a higher-quality, higher-performance electrode, paving the way for sustainable supercapacitor energy storage devices.

Acknowledgments The authors (RK and MP) are thankful to Indira Gandhi Delhi Technical University for Women (IGDTUW), Delhi, for providing the university JRF/SRF research for smooth ongoing research work in the RAMAN Lab. The authors thank the DST CURIE University Grant for research characterization facilities including FTIR and SEM in the parent institution.

Conflict of interest The authors declare that this work is original and has not been published elsewhere, nor is it currently under consideration for publication elsewhere. Further, we have no conflicts of interest to disclose.

References

- Z. Wu, L. Li, J. Yan, and X. Zhang, Materials design and system construction for conventional and new-concept supercapacitors. *Adv. Sci.* (2017). <https://doi.org/10.1002/advs.201600382>.
- M. Prajapati, V. Singh, M.V. Jacob, and C. Ravi, Recent advancement in metal–organic frameworks and composites for high-performance supercapatteries. *Renew. Sustain. Energy Rev.* 183, 113509 (2023). <https://doi.org/10.1016/j.rser.2023.113509>.
- T. Kwamman, S. Anantachaisilp, P. Limmeechokchai, and K. Kanjana, Enhancements of surface functional groups and degree of graphitization in gamma irradiated activated carbon as an electrode material. *Radiat. Phys. Chem. Phys. Chem.* 195, 110062 (2022). <https://doi.org/10.1016/j.radphyschem.2022.110062>.
- Q. Wang, Environmental science and opportunities. *Energy Environ. Sci.* 9, 729–762 (2016). <https://doi.org/10.1039/C5EE03109E>.
- D. Arvind and G. Hegde, Activated carbon nanospheres derived from bio-waste materials for supercapacitor applications—a review. *RSC Adv.* 5(107), 88339–88352 (2015). <https://doi.org/10.1039/C5RA19392C>.

6. S. Li, X. Tan, H. Li, Y. Gao, Q. Wang, G. Li, and M. Guo, Investigation on pore structure regulation of activated carbon derived from sargassum and its application in supercapacitor. *Sci. Rep.* 12(1), 10106 (2022). <https://doi.org/10.1038/s41598-022-14214-w>.
7. P.R. Kharangarh, Synthesis of luminescent graphene quantum dots from biomass waste materials for energy-related applications—an overview. *Energy Stor.* 1, 28 (2022). <https://doi.org/10.1002/est2.390>.
8. R. Kumari, P.R. Kharangarh, V. Singh, R. Jha, and C.R. Kant, Sequential processing of nitrogen-rich, biowaste-derived carbon quantum dots combined with strontium cobaltite for enhanced supercapacitive performance. *J. Alloys Compd.* (2023). <https://doi.org/10.1016/j.jallcom.2023.172256>.
9. S.M. Omokafe, A.A. Adeniyi, E.O. Igbafen, S.R. Oke, and P.A. Olubambi, Fabrication of activated carbon from coconut shells and its electrochemical properties for supercapacitors. *Int. J. Electrochem. Sci. Electrochem Sci* 15, 10854 (2020). <https://doi.org/10.20964/2020.11.10>.
10. S. Ghosh, R. Santhosh, S. Jeniffer, V. Raghavan, G. Jacob, K. Nanaji, P. Kollu, S.K. Jeong, and A.N. Grace, Natural biomass derived hard carbon and activated carbons as electrochemical supercapacitor electrodes. *Sci. Rep.* 9(1), 1–15 (2019). <https://doi.org/10.1038/s41598-019-52006-x>.
11. P. Tammela, A. Iurchenkova, Z. Wang, M. Strømme, L. Nyholm, and J. Lindh, Laser irradiation of photothermal precursors: a novel approach to produce carbon materials for supercapacitors. *ChemSuschem* (2024). <https://doi.org/10.1002/cssc.202301471>.
12. F. Barzegar, A. Bello, D.Y. Momodu, N. Manyala, and X. Xia, Effect of radiation on the performance of activated carbon based supercapacitor: Part I. Influence of microwave irradiation exposure on electrodes material. *Energy Procedia* 158, 4560 (2019).
13. N.S.M. Nor, M. Deraman, R. Omar, R. Farma, N.H. Basri, B.N.M. Dolah, N.F. Mamat, B. Yatim, and M.N.M. Daud, Influence of gamma irradiation exposure on the performance of supercapacitor electrodes made from oil palm empty fruit bunches. *Energy* (2014). <https://doi.org/10.1016/j.energy.2014.11.002>.
14. P. Numee, T. Sangtawesin, M. Yilmaz, and K. Kanjana, Activated carbon derived from radiation-processed durian shell for energy storage application. *Carbon Resour. Convers.* 7(2), 100192 (2024). <https://doi.org/10.1016/j.crcon.2023.07.001>.
15. R. Chaudhari and C.R. Kant, Highly stable and sensitive polystyrene/carbon black-BiI₃ composite for direct X-ray detector. *J. Mater. Sci. Mater. Electron.* 34(23), 1687 (2023). <https://doi.org/10.1007/s10854-023-11106-1>.
16. E. Adhamash, R. Pathak, Q. Qiao, Y. Zhou, and R. Mctaggart, Gamma-radiated biochar carbon for improved supercapacitor performance. *RSC Adv.* (2020). <https://doi.org/10.1039/d0ra05764a>.
17. R. Chaudhari, S.K. Sharma, C.R. Kant, and A. Garg, Investigations on low energy X-ray induced strong radiation-matter interaction phenomena in polymer-BiI₃ hybrid materials for room temperature radiation detectors. *Mater. Today Proc.* 67, 478 (2022). <https://doi.org/10.1016/j.matpr.2022.06.584>.
18. H.K. Maleh, İ.A. Kariper, C. Karaman, S. Korkmaz, and O. Karaman, Direct utilization of radioactive irradiated graphite as a high-energy supercapacitor a promising electrode material. *Fuel* 325, 124843 (2022). <https://doi.org/10.1016/j.fuel.2022.124843>.
19. T.R. Kumar and C.H.S. Chakra, Microwave-irradiated novel mesoporous nickel oxide carbon nanocomposite electrodes for supercapacitor application. *J. Mater. Sci. Mater. Electron.* 32(15), 20374 (2021). <https://doi.org/10.1007/s10854-021-06547-5>.
20. M. Kang, D. Heon, Y. Kang, and H. Jung, Electron beam irradiation dose dependent physico-chemical and electrochemical properties of reduced graphene oxide for supercapacitor. *Electrochim. Acta. Acta* 184, 427 (2015). <https://doi.org/10.1016/j.electacta.2015.10.053>.
21. A. Naidu, S. Dinda, V. Rao, A.V.R. Rao, T. Daida, and B. Radhika, Sustainable use of recycled soot (carbon black) for the cleaner production of value-added products: a compendium. *Chem. Eng. J. Adv.* 11, 100324 (2022). <https://doi.org/10.1016/j.cej.2022.100324>.
22. R. Kumari, V. Singh, and C.R. Kant, Enhanced performance of activated carbon-based supercapacitor derived from waste soybean oil with coffee ground additives. *Mater. Chem. Phys.* 305, 127882 (2023). <https://doi.org/10.1016/j.matchemphys.2023.127882>.
23. A. Tyagi, K. Mishra, and V. Kumar, Optimization of Sesamum indicum oil (sesame oil) derived activated carbon soot for electric double-layer capacitor (EDLC) application. *Biomass Convers. Biorefin.* (2023). <https://doi.org/10.1007/s13399-023-04121-z>.
24. G. Williams, M. Zankl, W. Abmayr, R. Veit, and G. Drexler, The calculation of dose from external photon exposures using reference and realistic human phantoms and Monte Carlo methods. *Phys. Med. Biol.* 31(4), 449 (1986).
25. Y. Zhang, Y. Zhao, L. Qiu, J. Xiao, F. Wu, and J. Cao, Diamond and related materials insights into the KOH activation parameters in the preparation of corn-cob-based microporous carbon for high-performance supercapacitors. *Diam. Relat. Mater. Relat. Mater.* 129, 109331 (2022). <https://doi.org/10.1016/j.diamond.2022.109331>.
26. Y. Lv et al., A comprehensive study on KOH activation of ordered mesoporous carbons and their supercapacitor application. *J. Mater. Chem.* (2012). <https://doi.org/10.1039/c1jm12742j>.
27. Saumya, K. Imtiyaz, M.A. Rizvi, and B.P. Nenavathu, Fabrication of graphitic carbon nitride/barium hydroxide nanocomposite as an effective anticancer agent against MCF-7 cell lines. *ChemistrySelect* 8(28), e202301710 (2023). <https://doi.org/10.1002/slct.202301710>.
28. A. Singh, S.K. Modi, P. Joshi, B.P. Nenavathu, M.S. Singh, S. Verma, and M.R. Hatshan, Sunlight mediated removal of toxic pollutants from Yamuna wastewater using efficient nano TeO₂-ZnO nanocomposites. *Chemosphere* 348, 140658 (2024). <https://doi.org/10.1016/j.chemosphere.2023.140658>.
29. R. Kumari, S.K. Sharma, V. Singh, and C.R. Kant, Facile, two-step synthesis of activated carbon soot from used soybean oil and waste engine oil for supercapacitor electrodes. *Mater. Today Proc.* 67, 483 (2022). <https://doi.org/10.1016/j.matpr.2022.07.253>.
30. S. Liu, P. Yang, L.W.Y. Li, Z. Wu, R. Ma, J. Wu, and X. Hu, Nitrogen-doped porous carbons from lotus leaf for CO₂ capture and supercapacitor electrodes. *Energy Fuels* 33, 6568 (2019). <https://doi.org/10.1021/acs.energyfuels.9b00886>.
31. H.B.M. Emrooz, M.S.H. Naghavi, S. Mohammadi, and S.M. Mousavi-Khoshdel, One-step green synthesis of meso-microporous carbons by self-activation of lemon wastes for high-performance supercapacitors. *J. Energy Stor.* 56, 105989 (2022). <https://doi.org/10.1016/j.est.2022.105989>.
32. E. Barsotti, S.P. Tan, M. Piri, and J. Chen, Capillary-condensation hysteresis in naturally-occurring nanoporous media. *Fuel* (2019). <https://doi.org/10.1016/j.fuel.2019.116441>.
33. R. Bardestani, G.S. Patience, and S. Kaliaguine, Experimental methods in chemical engineering: specific surface area and pore size distribution measurements—BET, BJH, and DFT. *Can. J. Chem. Eng.* 97(11), 2781–2791 (2019). <https://doi.org/10.1002/cjce.23632>.
34. V.S. Bhat, S. Supriya, and T.J. Jayeoye, Influence of surface properties on electro-chemical supercapacitors utilizing *Callerya atropurpurea* pod derived porous nanocarbons: structure property relationship between porous structures to energy storage devices. *Nano Select* (2020). <https://doi.org/10.1002/nano.202000013>.
35. M. Prajapati, C.R. Kant, S. Allende, and M.V. Jacob, Metal organic framework derived NiCo layered double hydroxide anode aggregated with biomass derived reduced graphene oxide cathode:

- a hybrid device configuration for supercapattery applications. *J. Energy Stor.* 73, 109264 (2023). <https://doi.org/10.1016/j.est.2023.109264>.
36. G.P. Ojha, B. Pant, J. Acharya, and M. Park, An electrochemically reduced ultra-high mass loading three-dimensional carbon nanofiber network: a high energy density symmetric supercapacitor with a reproducible and stable cell voltage of 2.0 V. *Nanoscale* 13(46), 19537 (2021). <https://doi.org/10.1039/D1NR05943B>.
37. A.A. Hor and S.A. Hashmi, Electrochimica acta optimization of hierarchical porous carbon derived from a biomass pollen-cone as high-performance electrodes for supercapacitors. *Electrochim. Acta* 356, 136826 (2020). <https://doi.org/10.1016/j.electacta.2020.136826>.
38. F. Barzegar, D. Momodu, F. Taghizadeh, D. Auret, N. Manyala, and X. Xia, Effect of radiation on the performance of activated carbon base supercapacitor: Part II. Influence of electron irradiation exposure on full cell. *Energy Procedia* 158, 4560 (2019). <https://doi.org/10.1016/j.egypro.2019.01.753>.
39. J.W. Graydon, M. Panjehshahi, and D.W. Kirk, Charge redistribution and ionic mobility in the micropores of supercapacitors. *J. Power. Sources* 245, 822 (2014). <https://doi.org/10.1016/j.jpowsour.2013.07.036>.
40. B.J. Choudhury, K. Roy, and V.S. Moholkar, Improvement of supercapacitor performance through enhanced interfacial interactions induced by sonication. *Ind. Eng. Chem. Res.* 60, 7611 (2021).
41. P.R. Kharangarh, V. Gupta, A. Singh, P. Bhardwaj, and A.N. Grace, An efficient pseudocapacitor electrode material with co-doping of iron (II) and sulfur in luminescent graphene quantum dots. *Diam. Relat. Mater.* 107, 107913 (2020). <https://doi.org/10.1016/j.diamond.2020.107913>.
42. M. Alzaid, F. Alsalh, and M. Zahir, Biomass derived activated carbon based hybrid supercapacitors. *J. Energy Stor.* 40, 102751 (2021). <https://doi.org/10.1016/j.est.2021.102751>.
43. P.R. Kharangarh, N.M. Ravindra, R. Rawal, A. Singh, and V. Gupta, Graphene quantum dots decorated on spinel nickel cobaltite nanocomposites for boosting supercapacitor electrode material performance. *J. Alloys Compd.* 876, 159990 (2021). <https://doi.org/10.1016/j.jallcom.2021.159990>.
44. B.A. Mei, O. Munteshari, J. Lau, B. Dunn, and L. Pilon, Physical interpretations of nyquist plots for EDLC electrodes and devices. *J. Phys. Chem. C* 122(1), 194 (2018). <https://doi.org/10.1021/acs.jpcc.7b10582>.

Publisher's Note Springer Nature remains neutral with regard to jurisdictional claims in published maps and institutional affiliations.

Springer Nature or its licensor (e.g. a society or other partner) holds exclusive rights to this article under a publishing agreement with the author(s) or other rightsholder(s); author self-archiving of the accepted manuscript version of this article is solely governed by the terms of such publishing agreement and applicable law.